Eur. Phys. J. E (2012) **35**: 21
DOI 10.1140/epje/i2012-12021-2

THE EUROPEAN PHYSICAL JOURNAL E

Regular Article

Structural and technical details of the Kirkwood-Buff integrals from the optimization of ionic force fields: focus on fluorides

M. Fyta[a]

Physics Department (T37), Technical University of Munich, 85748 Garching, Germany and
Institute for Computational Physics, University of Stuttgart, 70569 Stuttgart, Germany

Received 13 december 2011 and Received in final form 1 March 2012
Published online: 22 March 2012 –

Abstract. Results on the structural details of Kirkwood-Buff integrals obtained from the optimization of ionic force fields are presented. We have proposed and make use of an optimization scheme for ionic force fields, which is based on the modification of the cation-anion mixing rules, the calculation of the thermodynamics properties of various monovalent salt solutions according to the Kirkwood-Buff theory of solutions and the comparison to relevant experimental findings. Here, we complete and extend our calculations and analysis as we focus on the technical details of this optimization procedure and the case of fluorides, which have been proven difficult to handle. Important insight is given on the dependence of the radial distribution functions, the short-ranged potentials of mean force, and the Kirkwood-Buff integrals of the salt solutions on the different scaling factors in the mixing rules. Specifically, the way the structural details and inherent characteristics of the above properties are affected by the quantitative and qualitative differences in the mixing rules for a variety of common biologically relevant monovalent salts is mainly addressed. We conclude on the efficiency of this scheme, again with a focus on the fluorides. In the end, we provide a variation of the ion-pair mixing rules scaling factors with salt concentration to identify regimes for which different mixing rules prefactors lead to well-optimized force fields. All results are obtained through Molecular Dynamics simulations using previously optimized force fields for the monovalent ions.

1 Introduction

The quest for well-optimized classical ionic force fields is a subject of intense research over the last years [1–3]. These can be combined with classical atomistic simulations to model ionic solutions [4], also in the context of biomolecules [5,6]. Classical ionic force fields may not be as accurate as quantum-mechanical–based ones, they are though computationally less demanding. In this respect, classical simulations can span larger spatial and temporal scales than quantum-mechanical ones. Commonly, classical pairwise additive non-polarizable ionic potentials keep the parameter space small and are combined with explicit water models, without any additional assumptions on the solvent-mediated forces involved in the system [7,8]. Within such a scheme, the atoms are characterized by partial Coulombic point charges, excluded-volume sizes, and dispersion attractions. Specifically, for obtaining pairwise ionic potentials, various optimization schemes have been proposed over the years, some of which are based on single-ion properties [9, 10]. Others take into account ion-pair properties [11], for which a typical approach is the calculation of the thermodynamic properties of the salt solutions [2, 12] and the comparison to relevant experimental data. A good comparison results in well-optimized potentials for ions in solution. In the end, the question that always arises is how transferable the derived ionic force fields are.

A method that has been recently proven efficient for the optimization of pairwise additive ionic potentials is the Kirkwood-Buff theory of solutions (KBT) [13]. The Kirkwood-Buff integrals are directly related to the structural details of the ionic solutions and can be mapped to relevant experimental observations. KBT has been often used before to realize the solution thermodynamics of mixtures of various cosolutes and ions with water [14–18]. In a two-component system, like monovalent salt solutions in water, the derivation of properties such as the activity derivatives of the solutions is straightforward [2, 19]. Such an approach has recently been used together with modified ion-pair mixing rules [19]. Within that approach the cation-water mixing rules have not been modified as in similar studies [2,20,21], since the bare water-ion interactions are not expected to change due to the presence of other ions.

[a] e-mail: mfyta@tum.de; mfyta@icp.uni-stuttgart.de

We extend here our calculations and the analysis of the ion force field optimization scheme based on the KBT and the cation-anion modified combination rules we have previously proposed [19]. In our previous work, we had separately modified either the cation-anion interaction term or the cation-anion effective radius for a series of monovalent salt solutions. Here, we look deeper into more technical details, such as the connection of the scaling prefactors in the combination rules to the structural details of the Kirkwood-Buff integrals of the solutions or the potentials of mean force for the ion-pairs. We look again briefly at various salt solutions, but focus more on two of the fluorides, NaF and KF. We had previously shown that in some cases, such as KF, the modification of the cation-anion effective radius can be proven more efficient for the optimization of the corresponding ionic force fields. We investigate whether the trends we observed are common to other salts as well, using NaF as another probe. As a final remark on the transferability of the ionic force fields for fluorine, we look at the concentration dependence of the activity derivatives obtained through our calculations and compare to the relevant experimental data.

The paper is organized as follows: in sect. 2, we present the methodology used in this study and the force field parameter space entering our simulations. In sect. 3 we discuss the structural and interaction details of the ionic solutions, and the corresponding Kirkwood-Buff integrals, as well as the effect of the scaling prefactors in the combination rules specifically for two of the fluorides. We summarize our conclusions in sect. 4.

2 Methods

2.1 Molecular Dynamics simulations

We perform atomistic Molecular Dynamics (MD) simulations, using GROMACS as the simulation package [22,23]. All calculations are done within the (N, P, T) canonical ensemble, for which the particle number N is constant, as well as the pressure $P = 1\,\text{bar}$ and temperature $T = 300\,\text{K}$. We have used a Berendsen barostat and thermostat [24] and a cubic simulation box with an edge length of $L = 4\,\text{nm}$, which is periodically repeated in all three dimensions. The initial ionic configurations are generated from the cubic box of equilibrated water molecules by randomly replacing those molecules and inserting ions until the desired concentration is reached. Our MD simulations include explicit ions and SPC/E water [25], within which oxygen and hydrogen atoms are connected by rigid intramolecular bonds and carry partial charges. The initial total number of water molecules was 2180. The three-dimensional particle-mesh Ewald sum was used as a summation method for the electrostatics [26], employing a grid spacing in Fourier space of 0.12 nm in all three directions. The interpolation we have used is of the order of 4 together with a distance cutoff of 0.9 nm for the real-space interactions, and a cutoff of 10^{-5} for the relative strength of the electrostatic interaction. The typical MD simulation time was in the range of 100–150 ns. We have looked at the NaCl, NaBr, NaI, KCl, CsCl, and CsI salt solutions and focused specifically on KF and NaF. A typical concentration used is 0.3 m (mol/kg) corresponding to about 0.3 M (mol/l). In this case, the water box includes 12 anions and 12 cations. For the variation with concentration we vary the number of anions and cations. The initial cubic simulation boxes for each salt solution and varying concentration were generated by randomly placing water molecules with ions starting again from pure solvent boxes of a length between 4 nm and 6 nm.

2.2 Ionic potentials and mixing rules

In the MD simulations, the ions are modeled as charged and non-polarizable spheres. A 6-12 Lennard-Jones (LJ) potential is used here to model the interactions between the ions. The non-electrostatic interaction for atoms i and j at a distance r_{ij} is modeled by a pairwise Lennard-Jones (LJ) interaction of the form

$$V_{\text{LJ}}(r_{ij}) = 4\varepsilon_{ij}\left[\left(\frac{\sigma_{ij}}{r_{ij}}\right)^{12} - \left(\frac{\sigma_{ij}}{r_{ij}}\right)^{6}\right]. \quad (1)$$

For each pair of atoms or ions, there are two free parameters, the effective radius σ_{ij} and the interaction term ε_{ij}. For the SPC/E water used in our simulations, the LJ parameters are $\varepsilon_O = 0.6500$ (kJ/mol) and $\sigma_O = 0.3169$ (nm) and are assigned only to the oxygen molecule of water, without any parameters related to the two hydrogen atoms. A charge of $q_O = -0.8476q/e$ and $q_H = +0.4238q/e$ is assigned to the oxygen and hydrogen atom of the water molecule, respectively [25]. Typically, for the cross interactions ($i \neq j$) in the LJ potential, mixing rules are used. The common mixing rules are $\varepsilon_{ij} = \sqrt{\varepsilon_{ii}\varepsilon_{jj}}$, and either $\sigma_{ij} = (\sigma_{ii} + \sigma_{jj})/2$, defining the Lorentz-Berthelot (LB) mixing rules, or $\sigma_{ij} = \sqrt{\sigma_{ii}\sigma_{jj}}$, forming the geometric mixing rules [27].

The Lorentz-Berthelot combination rules are used here. We have efficiently used these in similar studies for the calculation of thermodynamic properties of salt solutions [12,19]. It was also previously shown that including an additional scaling prefactor in the ionic mixing rules can more adequately describe single-ion properties and ion-pairing properties [2,19,20]. In this respect, we choose a triplet of optimized properties $\{\sigma, \varepsilon, \lambda_k\}$, where k stands for ε or σ. The scaling factors λ_ε and λ_σ are introduced for the LJ parameters according to $\varepsilon_{+-}{=}\lambda_\varepsilon\sqrt{\varepsilon_{++}\varepsilon_{--}}$ and $\sigma_{+-}{=}\lambda_\sigma(\sigma_{++} + \sigma_{--})/2$, which describe deviations from the usual Lorentz-Berthelot mixing rules. Only the ion-pair mixing rules are modified. As the determination of ion-water interaction parameters from single-ion properties was quite robust, we did not modify the ion-water interaction parameters as was done in previous KBT modelling studies [2,20,21].

Table 1. Parameters for the LJ potential for the ions studied in this work. The parameters for Na^+, Cl^-, and Br^- are taken from refs. [28,29]; the rest from ref. [12].

	Na^+	K^+	Cs^+	$F4^-$	$F5^-$	Cl^-	Br^-
σ_{iO} (nm)	0.2876	0.293	0.333	0.3665	0.38	0.3785	0.39
ε_{iO} (kJ/mol)	0.5216	1.26	0.5	0.1	0.041	0.5216	0.52

2.2.1 LJ parameter space for the ions

For all ions considered in this work, we have used the optimized LJ parameters and λ_k scaling prefactors from our previous studies [12, 19]. The LJ parameters for the ions lie on the free energy of solvation curve for single ions [10] and reproduce the ionic radius with acceptable accuracy. For sodium (Na^+), chlorine (Cl^-), and bromine (Br^-) we take the parameters given by Dang [28,29]. These give reasonable hydration free energies [9, 10] and are consistent in determining thermodynamic properties [20,30]. For F^-, which has been proven problematic [10,12,30], we use our previously optimized force field (labeled F5 in table 1), as well as an additional force field with a small LJ interaction energy (labeled F4 in table 1), for comparison [12]. All Lennard-Jones ion-water parameters, ε_{iO} and σ_{iO}, used in this work are summarized in table 1. Note, that the subscripts iO denote the parameters between ion and water (the oxygen atom of the SPC/E water model). For consistency, the numbers in parentheses for fluorine follow our previously used notation [12].

The procedure we have followed here for the optimization of ionic force fields is the following [19]: for each salt, we vary the scaling factor λ_k and obtain the structural details, mapped through the radial distribution function of the solution. We then calculate the Kirkwood-Buff integrals (KBIs) for the solution, which lead us to the activity derivatives, as will be outlined below. The optimized λ_k for each salt solution is obtained by comparing the calculated activity derivatives to the respective experimental measurements (the index k again denotes either ε or σ). From our previous investigation, we have concluded to the following λ_ε values which lead to a good comparison to the experimental data [19]: λ_ε=1.5, 1.0, 1.0, 0.9, 1.0, 1.0, 1.0, 1.0 for NaF5, NaCl, NaBr, NaI, KF5, KCl, CsCl, and CsI, respectively. F5 denotes the respective force field for fluoride in table 1. For KF5, λ_ε=1.0 is the optimum value, but again does not provide a very good comparison to the experimental observations. For KF5 then, we also obtained a better comparison by modifying the σ_{+-} parameter with λ_σ=1.55 leading to properties that approach the experimental results. We next look at the effect of the different λ_k values on the structural details of the radial distribution functions (RDFs), the short-ranged potentials of mean force, and the various contributions to the KBIs.

2.3 Structural analysis

2.3.1 Radial distribution functions

The electrolyte structural properties of the salt solutions can be effectively monitored through the RDFs ($g_{ij}(r)$) which are directly obtained through the MD simulations. The RDF describes how the atomic density varies as a function of the distance r from one particular atom. Finite-size corrections need first to be taken into account for the RDFs, which should reach unity at long distances. These effects are demonstrated by an erroneous normalization of the simulated rdfs, $g_{ij}^{\rm sim}(r)$ [31]. In order to overcome this, a correcting factor is introduced, so that the corrected RDF used in the calculations of the KBIs is written as $g_{ij}(r;\rho) = f(\rho)g_{ij}^{\rm sim}(r';\rho)$. The prefactor $f(\rho)$ depends on the solution concentration ρ and is of the order of $1 \pm 1/N_s$. According to our simulations, for most salt solutions considered here, the "+" sign is observable for the correction of the cation-anion g_{+-}, while the "−" sign for the rest.

2.3.2 Short-ranged potentials of mean force

As a probe of the local interactions in the salt solutions, we also look at the short-ranged potentials of mean force, following an approach previously used in electrolyte studies [30]. The potential of mean force $w_{ij}(r;\rho)$ at density ρ results from the RDF through a Boltzmann inversion [32, 33] and can be decomposed into a short-ranged ($w_{ij}^{\rm sr}(r;\rho)$) and a long-ranged contribution [34]. The long-ranged part of the potential of mean force is a non-specific Debye-Hückel potential and can be subtracted from $w_{ij}(r;\rho)$ leading in this way to the short-ranged part of the pair potential

$$w_{ij}^{\rm sr}(r;\rho) = w_{ij}(r;\rho) - w_{ij}^{\rm DH}(r;\rho). \tag{2}$$

In the low density limit, the potential of mean force between two ions reduces to their effective pair potential and the decomposition can be written as the short-ranged part of the pair potential, $V_{ij}^{\rm sr}(r)$, and the usual Coulombic part

$$\beta V_{ij}^{\rm eff}(r) = \beta V_{ij}^{\rm sr}(r) + z_i z_j \lambda_B(0)/r, \tag{3}$$

where $\beta = 1/k_BT$ is the inverse thermal energy, z_i, z_j are the valencies for the two ion types, respectively, and $\lambda_B(\rho)$ is the concentration-dependent Bjerrum length. $V_{ij}^{\rm sr}$ can be derived through the finite concentration potential of mean force, $V_{ij}^{\rm sr}(r) \simeq w_{ij}^{\rm sr}(r;\rho)$. This procedure works well for RDFs generated at a finite concentration of $\rho \simeq 0.3$ M, as the one considered in this work. We should also note that, though not exactly correct, the non-specific Debye-Hückel potential is often used for the derivation of effective potentials. Nonetheless, the Debye-Hückel decay corresponds to the Debye-Hückel length only for highly dilute solutions.

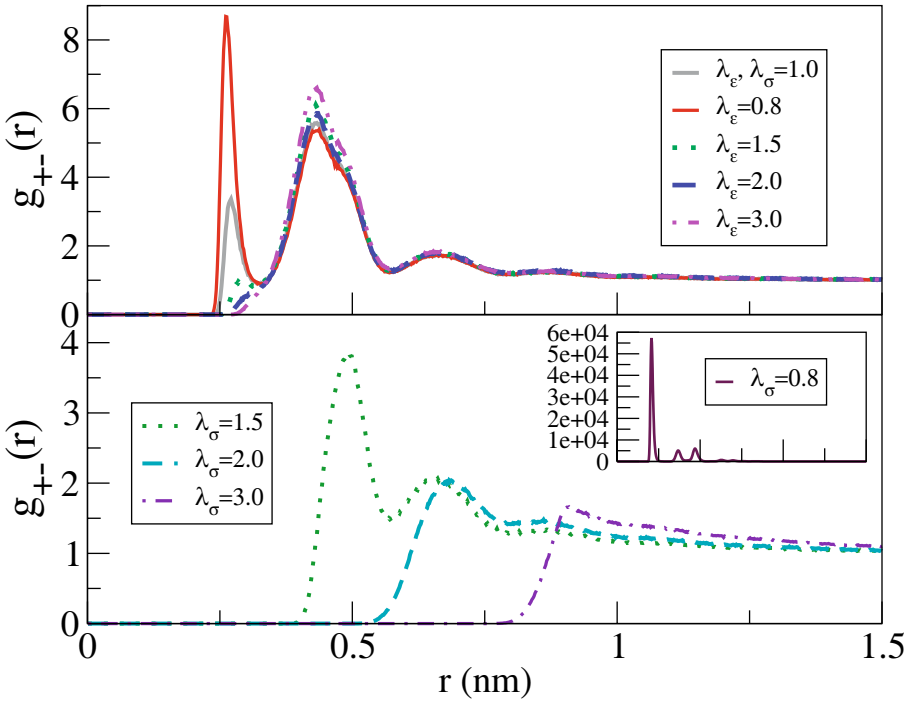

Fig. 1. Cation-anion RDFs for the KF5 solution at 0.3 m (0.3 M). The data are shown as a variation of the λ_ε (upper panel) and the λ_σ (lower panel) scaling factors, respectively.

For dilute or concentrated solutions, the screening parameter and, thus, this "Debye-Hückel" term depends on the nature of the ions. Additional details on the derivation of the short-ranged potentials of mean force can be found elsewhere [12, 30].

2.3.3 Kirkwood-Buff integrals and activities

The macroscopic thermodynamics of a solutions can be linked to its microscopic structure through the Kirkwood-Buff theory of solutions [13], which is described by the Kirkwood-Buff integrals (KBIs). The KBIs are directly obtained from the structural details (the RDF) of the solution. Let $g_{ij}(r)$ be the RDF (or pair correlation function) between species i and j at a distance r. The KBIs for these two species can be defined as

$$G_{ij} = \int_0^\infty 4\pi r^2 [g_{ij}(r) - 1] \mathrm{d}r. \tag{4}$$

Here, we handle the electrolyte solution as a binary system of water (w) and cosolvent (c) [14,35]. In this respect, the relevant KBIs related to the thermodynamic properties of the solution are G_{ww}, G_{cc}, and $G_{cw} = G_{wc}$.

As a probe of the solution thermodynamics, we calculate the activity derivatives (a_{cc}) of the solution, which can be mapped directly to the experimental electrolyte activity a_c. This in turn is connected to the molar activity coefficient y_c, where $a_c = y_c \rho_c$. In this expression, $\rho_c = N_c/V$ is the cosolvent number density, N_c the number of cosolvents, and V the volume. At a constant temperature (T) and pressure (P), a_{cc} and a_c can be derived through the KBT, according to the equations

$$a_{cc} = \frac{1}{1 + \rho_c (G_{cc} - G_{cw})}, \tag{5a}$$

$$a_{cc} = \left(\frac{\partial \ln a_c}{\partial \ln \rho_c}\right)\Big|_{P,T} = 1 + \left(\frac{\partial \ln y_c}{\partial \ln \rho_c}\right)\Big|_{P,T}. \tag{5b}$$

The cosolvent-water and cosolvent-cosolvent components of the KBIs involved in the above equations are given by $G_{cw} = (G_{w+} + G_{w-})$ and $G_{cc} = \frac{1}{4}(2G_{+-} + G_{++} + G_{--})$. Additional details on the KBT for ionic solutions can be found elsewhere [2, 14, 19, 35].

3 Results and discussion

3.1 RDFs, short-ranged potentials, and mixing rules

We begin the analysis with the cation-anion RDFs ($g_{+-}(r)$) for the KF and NaF solutions. We have used two different F^- force fields, F4 and F5 shown in table 1 and compare overall the different features of these force fields for the two fluorides, KF and NaF and the different scaling prefactors. We first look at the cation-anion RDF for the KF5 solution, for which the F5 force field was used. The results are depicted in fig. 1 and show a clear tendency with the scaling prefactor λ_k. Specifically, the smaller λ_ε the higher the first contact peak, which becomes too high for even smaller values of λ_ε (data not shown) denoting ion-pair crystallization. As λ_ε increases above 1, the first

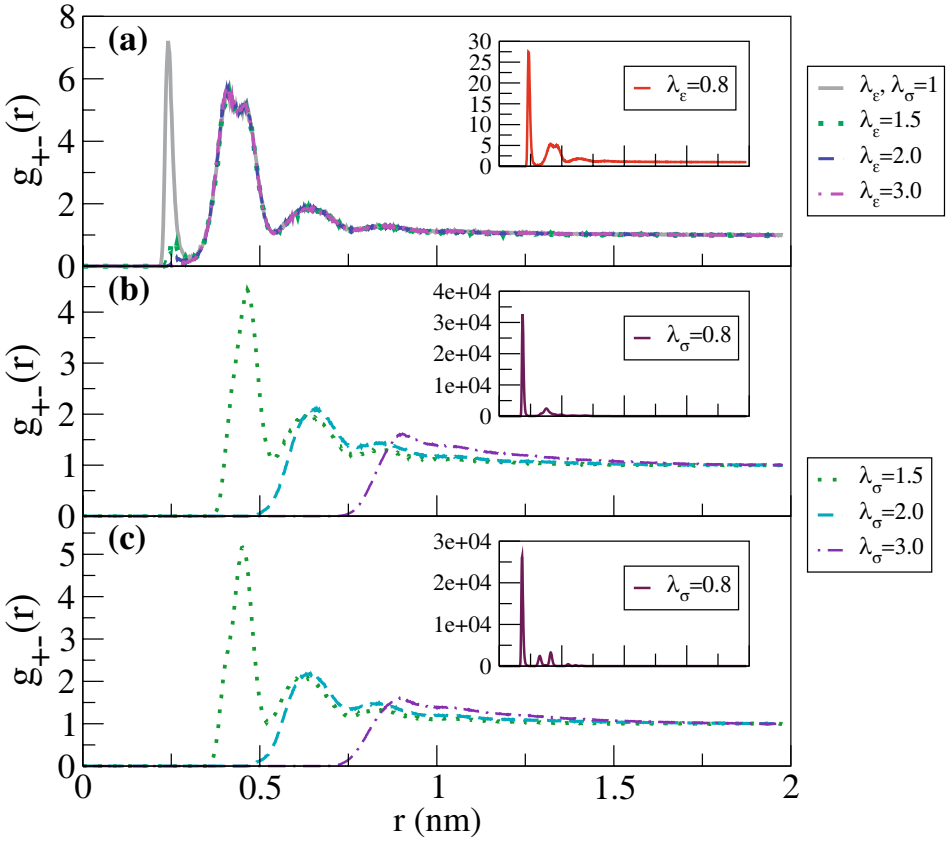

Fig. 2. Cation-anion RDFs for the NaF5 solution at 0.3 m (0.3 M). The data are shown as a variation of (a) the λ_ε and the (b) λ_σ scaling factors, respectively. As a comparison the RDFs for the NaF4 solutions are also shown in panel (c) as a variation with λ_σ.

ion-pair contact peak decreases, becoming almost negligible for λ_ε=2, while the second solvent-separated ion-pair peak becomes higher (upper panel of the figure). A close look at the lower panel of fig. 1 reveals a similar decrease in the first contact peak when σ_{+-} is varied. The peak is simultaneously shifted towards larger ion-pair distances. For λ_σ=3 this peak has almost diminished, while no second contact peak is evident, revealing a much different bonding environment when the ion-pair effective radius becomes large.

The trends are similar for the NaF solution, the RDFs of which are shown in fig. 2. The crystallization for NaF is more clear for scaling prefactors below 1. In this case, though, the second contact peak does not seem to be affected as λ_ε is increased (panel (a)). In panel (c), we also show the RDFs for NaF4 for the F4 force field as a variation of the λ_σ factor. In essence, the difference in the RDFs compared to the NaF5 case (panel (b)) are nailed down to a slight shift along the ion-pair distance: the RDFs for NaF5 are shifted to about 0.01 nm to the left of those for NaF5. Turning to the short-ranged potential of mean force for NaF4 and NaF5 in fig. 3, we identify a continuously shallower first minimum as λ_ε decreases, denoting a smaller attraction, while the second minimum is kept almost intact. In the variation with λ_σ in panel (b) of the same figure, the first potential well again becomes shallower, denoting less attraction as the prefactor is increased, and the whole potential curve becomes almost flat for $\lambda_\sigma > 2$. A very similar situation is inspected also for NaF4 in panel (c), which is shown as a comparison. Here, the differences between the NaF4 and NaF5 solutions are qualitatively a bit larger than those observed in the respective RDFs. It will be later shown that these relatively small differences lead to larger deviations in the respective KBIs and activity derivatives.

3.2 Structural details of the Kirkwood-Buff integrals

We now move on to the investigation of the various contributions to the Kirkwood-Buff integrals. First, we look at the G_{ij} values, with i, j, being + for the cation, − for the anion, and w for the water part. The results for all salts considered here are summarized in fig. 4(a). In this figure, the different values of the KBIs with respect to λ_ε are provided. As a first remark, G_{+-} is always positive, G_{++} and G_{--} negative, while G_{w+} and G_{w-} very small (typically of the order of 10^{-2}) and either slightly negative or slightly positive. It is also clearly visible in this figure that, for λ_ε <1, large deviations in the KBI values occur, while for $\lambda_\varepsilon \geq 1$, the KBIs do not change significantly. This fact is again connected to the tendency for crystallization of the ions for λ_ε <1. In this respect, a recipe for obtaining

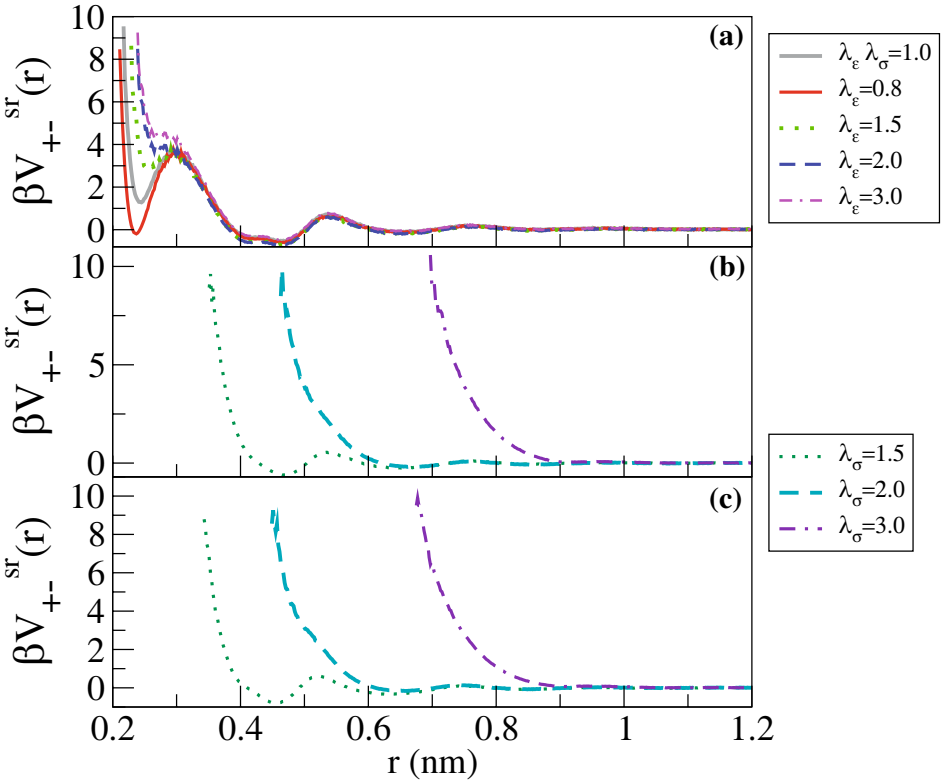

Fig. 3. Cation-anion short-ranged potentials of mean force for the NaF solution at 0.3 m (0.3 M). The data are shown as a variation of (a) λ_ε and (b) λ_σ, respectively, for the F5 force field. In (c) similar results are shown for the F4 force fields as a function of λ_σ.

good λ_ε scaling factors, thus, well-optimized force fields, could be based on these technical features: large (over $\approx$ 3-4) G_{+-} values, positive G_{++} and G_{--}, and absolute values of G_{w+}, G_{w-} larger than 10^{-1}, cannot lead to well-optimized ionic force fields. This is meant in the sense that the corresponding thermodynamic properties, such as the activity derivatives, do not compare well to the relevant experimental data, as will be shown in the following.

We also take a look at the G_{cc} and G_{cw} contributions for the NaF and KF solutions and the two different force fields F4, F5. The results with respect to either λ_ε or λ_σ are given in fig. 4(b). Here, G_{cc} needs to be positive and of the order of 1 and G_{cw} of the order of 10^{-2} and either positive or negative, in order to get a good comparison between our MD simulations and experiments, as mentioned above. Again, deviations from a good comparison occur mainly for λ_k <1, which again denotes crystallization and unphysical behavior. Note here that the phase transition observed for these small λ_k values is actually related to the electrostatic energy of the ions at contact. This can be analytically evaluated as was shown by recent MD simulations of ionic solutions [36, 37]. The variations between the two F^- force fields are not that significant. More or less the respective curves vary similarly. A significant difference, though, is seen in G_{cc} when comparing the NaF5 and KF5 solutions under a variable σ_{+-}. This difference, inherent in the KBI contributions is very likely the reason why using the λ_ε leads to well-optimized force fields for NaF, but not for KF, when the F5 force fields is used [19]. We will return to this issue in the following.

An additional insight to the differences between the two fluorides and the two F^- force fields is given through the variation of the G_{cc} and G_{cw} KBIs with the cosolvent-cosolvent or cosolvent-water distance, respectively. The results are shown again for various λ_ε and λ_σ values in fig. 5. The data for KF5 and NaF5 in panel (a) show some interesting features. First, the structure of the G_{cc} and G_{cw} curves for λ_ε and λ_σ differ, denoting the different bonding and hydration environment in these cases. The deviations among the curves for the same values of λ_ε and λ_σ are larger for the latter case. These deviations are more significant for the G_{cc} case, revealing the importance of the cosolvent-cosolvent interactions in the whole optimization procedure. Overall large deviations in this picture are evident in the case of crystallization (*e.g.*, for $\lambda_\sigma < 1$). This is also obtained through the comparison of KF4 and KF5 in fig. 5(b). Curves for $\lambda_\sigma < 1$ correspond to crystallization and unphysical (too attractive) cation-anion interaction, thus very large absolute values of G_{cc} and G_{cw}. When λ_ε is varied, both G_{cc} and G_{cw} curves corresponding to the F4 force field are increased with respect to the F5 one. This is directly related to the corresponding higher contact peaks in the RDFs for KF4 as compared to KF5 (data not shown). On the other hand, when λ_σ is varied the differences between the KBI curves for KF4 and KF5 are less significant. This is again justified from a closer look to the

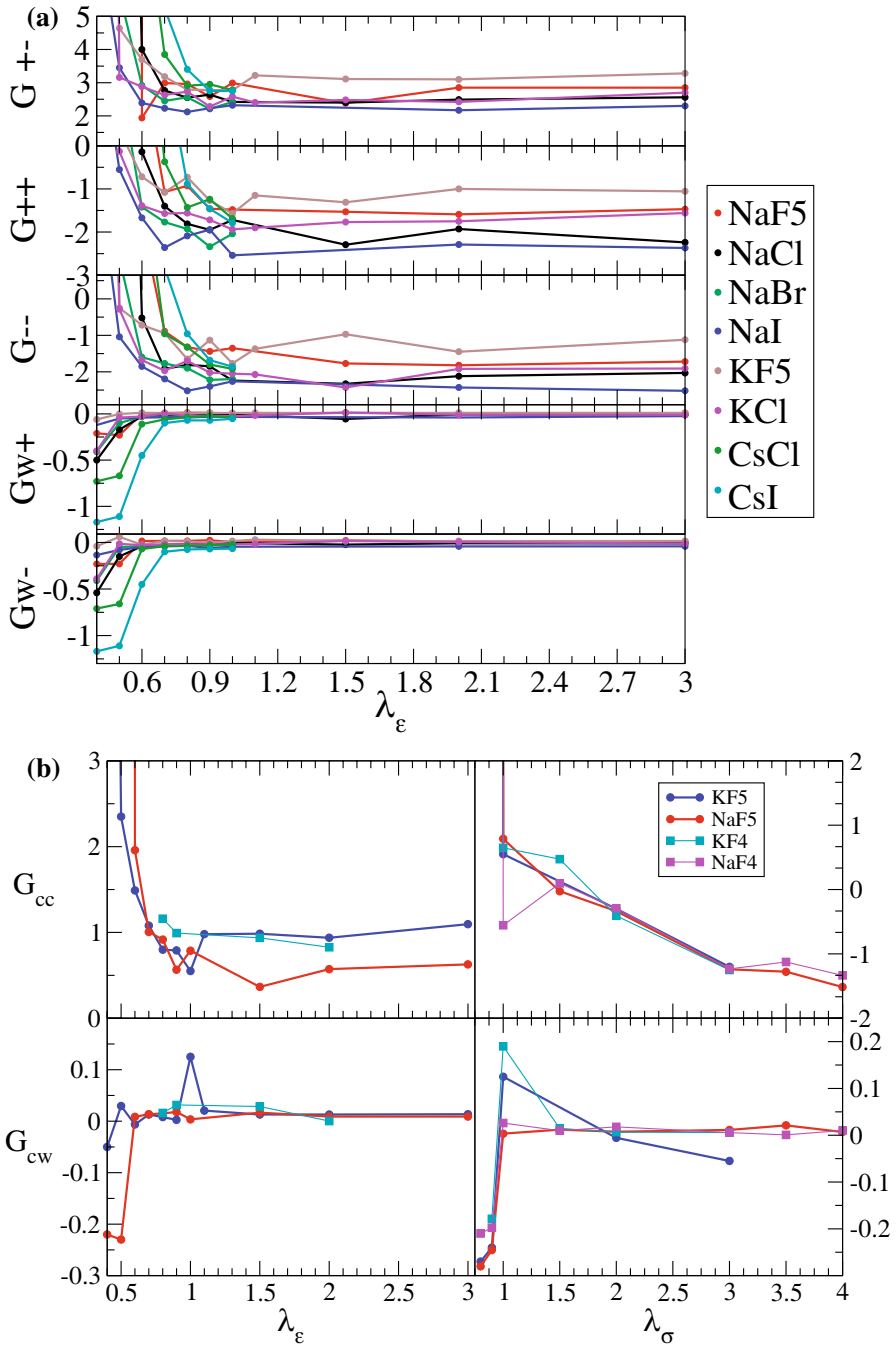

Fig. 4. (a) The Kirkwood-Buff integral values of the different contributions for all the salts considered in this work at 0.3 m (0.3 M) solution. Labels +, −, and w denote the cation, anion, and water contribution, respectively. (b) Kirkwood-Buff integral values of G_{cc} and G_{cw} for the KF5 and NaF5 solutions (at 0.3 M). The results are shown with respect to the scaling factors in the mixing rules, λ_ε and λ_σ, respectively. The results for the KF4 and NaF4 salts are also shown as a comparison.

respective RDFs, the respective curves of which are very similar apart from a very slight shift (of the order of 0.02) in the cation-anion distance (data also not shown).

3.3 Activity derivatives

We have previously shown that for KF scaling the ion-pair LJ interaction does not lead to a good comparison of the thermodynamic properties to the relevant experimental data, hence not a well-optimized force field. This was resolved by scaling the ion-pair LJ effective radius instead [19]. Here, we investigate whether indeed modifying the σ_{+-} LJ parameter is a better optimization procedure also for other salts and take NaF as a probe. Following the derivation of the activity derivatives according to eq. (5a), we present in fig. 6 the activity derivatives for

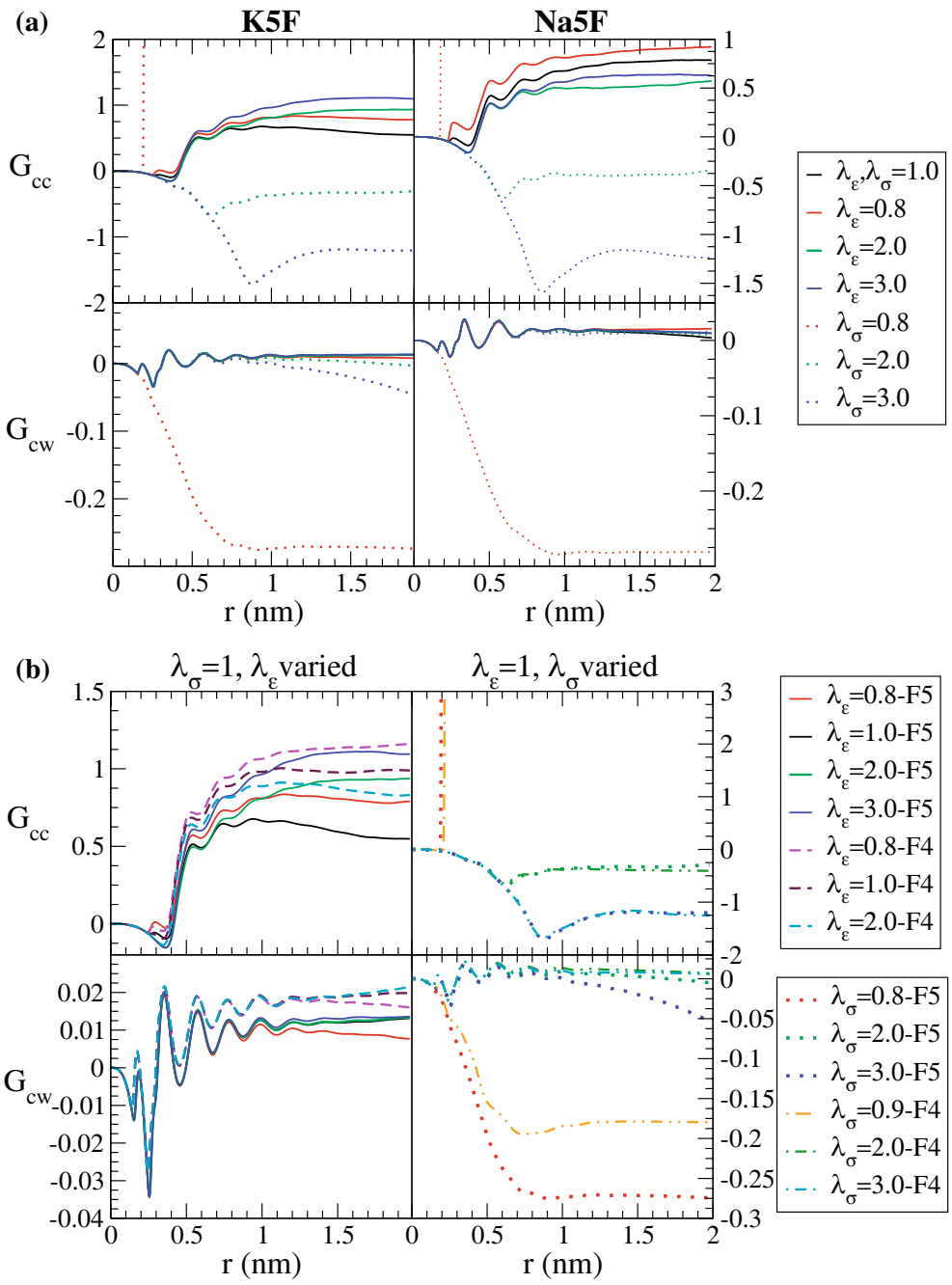

Fig. 5. (a) Kirkwood-Buff integrals (G_{cc} and G_{cw}) for (a) the KF5 and NaF5 solutions and (b) for the KF5 and KF4 solutions. All results are shown for different values of the scaling factors in the mixing rules, λ_ε and λ_σ, respectively, at a concentration of 0.3 m (0.3 M). The labels in the legend denote which F^- force field is used.

NaF. The error in the calculation of the activity derivatives is estimated through the block averaging method at about ±0.03 and is also shown in the figure. The experimental activities shown as a function of molality are obtained from [38]. The results are shown for solutions at a 0.3 m concentration. In this figure, we compare both force fields F4 and F5 and both ways of modifying the mixing rules (λ_ε and λ_σ). We first look at NaF5, for which values $\lambda_\sigma < 1$ lead to ion clustering and almost negligible activity derivatives. Interestingly, similar to the KF case [19], increasing λ_σ increases the activity derivatives. There is a definite crossover with the experimental line around $\lambda_\sigma = 1.2$–1.3. The behavior of NaF4 is quite similar. The data for NaF5 as a function of λ_ε and fixed $\lambda_\sigma = 1$ are also shown for comparison. In this case, the calculated a_{cc} values for $\lambda_\varepsilon \geq 1$ are close, but almost always below the experimental line. In this figure, it is clearly seen that the scaling factor λ_σ for the cation-anion LJ diameter σ_{+-} term can also be a very efficient alternative to the λ_ε scaling factor, also in cases where the latter factor

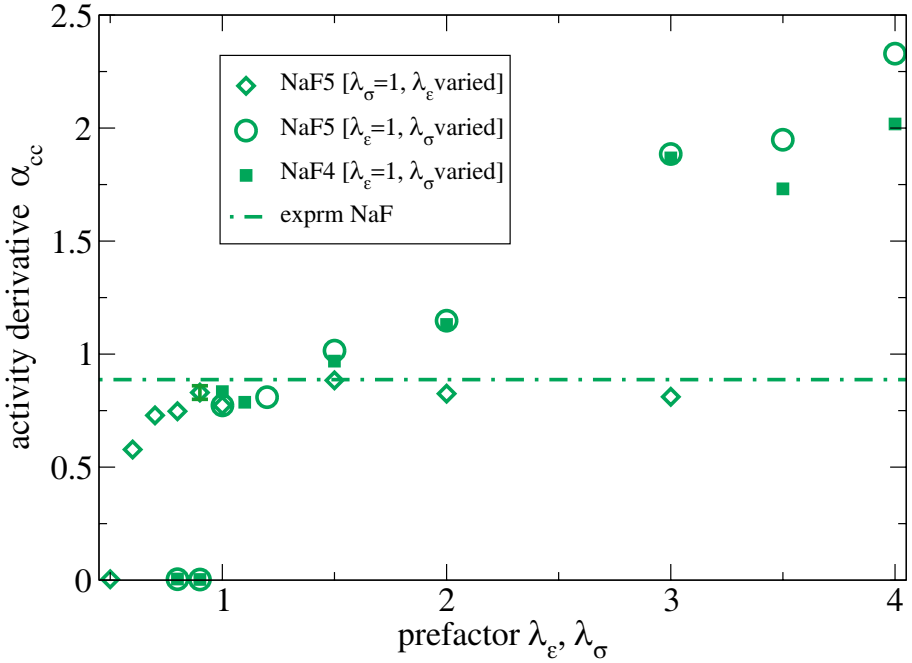

Fig. 6. Activity derivatives a_{cc} for the NaF solutions as a function of the scaling factors λ_ε and λ_σ. Note that only one of the factors is varied, the other is fixed at unity. The line shows the respective experimental value. The error bar is shown only for one data point for clarity, but should be similar for all data points. The ionic concentration is 0.3 m (0.3 M).

does not fail. This allows the derivation of more than one well-optimized ionic force fields, which can possibly be applied alternatively to different systems. It is, thus, evident that not only for the other salt solutions modeled in this study, but also for the variety of ions that need a good force field, both optimization schemes, modifying ε_{+-} or σ_{+-}, can be sufficient.

As a supplementary information of the above conclusion, we show in fig. 7 the efficiency of the two optimization schemes (modified ε_{+-} or σ_{+-}). Modifying ε_{+-} for all salt solutions considered in this work leads to the results shown in panel (a) of this figure, which correspond to the optimized λ_ε values given in sect. 2.2.1. The MD activity derivatives are compared to the experimental ones, revealing a very good agreement, apart from the KF case. In panel (b) of the same figure, we compare the two fluoride force fields and the two optimization schemes for the NaF and KF solutions. The data shown correspond to various values of the scaling prefactors. The optimum prefactors are also depicted, namely λ_σ=1.55, 1.5, 1.0, and 1.0 for KF5, KF4, NaF5, and NaF4, respectively, and λ_ε=1.0, 1.5 for KF4 and NaF5. It is clearly shown that the activity derivatives for both KF4 and KF5 are improved when σ_{+-} is modified instead of ε_{+-}. For NaF varying ε_{+-} can also be quite efficient and gives a_{cc} values close to the experimental ones. Note, though, that the data shown in fig. 7(b) are only indicative of a trend. As there is a crossover with the experimental lines for both NaF and KF when modifying σ_{+-}, calculation of the activity derivatives for λ_σ values exactly at the crossing points will shift the respective data in fig. 7(b) very close to the experimental lines. Specifically, a_{cc} continuously increases with increasing λ_σ, while the respective curves when varying λ_ε usually saturate just below the experimental line, as the ion-pair is trapped in a local minimum of the interaction potential [19]. This is also indicated by the different λ_k values shown for each salt in this figure. For most of the cases, all the λ_ε lead to activity derivatives lower than the experimental lines, while increasing λ_σ should also lead to a_{cc} values that can match the experimental data.

3.4 Transferability dependence on ionic concentration

Finally, we briefly address the issue of transferability, which is always a critical question when generating new force fields. We have already shown, for example, that the F4 and F5 LJ parameter sets can in principle be quite efficient for both KF and NaF, provided that the optimum values for either λ_ε or λ_σ are used. In general, force field transferability can be addressed in terms of the variety of systems the derived force field can be applied to; systems different than the one for which the force field has been generated. The transferability can also be checked for different conditions than the ones used for the force field optimization. Here, we choose this latter case and investigate the concentration dependence of the activity derivatives. We study this dependence for one of the salt solutions modeled here as a representative case. The KF5 solution has been chosen, which was a problematic case in this and a previous study [19]. Note, that the activity derivative describes, in principle, the change in the activity (chemical potential) of the salt with concentration. The results

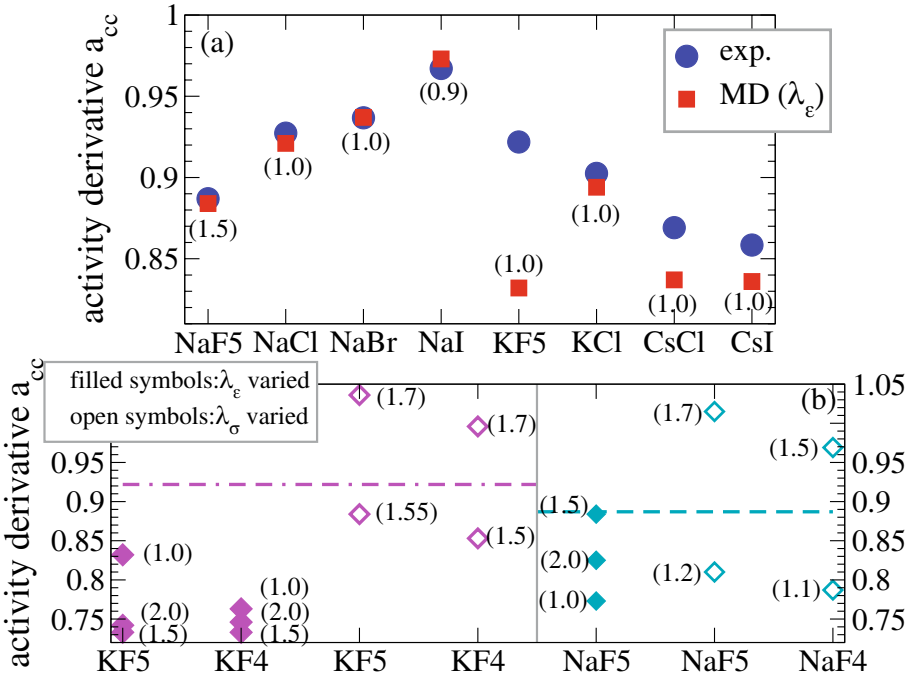

Fig. 7. (Color online) Activity derivatives a_{cc} for the salt solutions considered in this work. In (a) the data from the simulations (MD) are shown in comparison to the respective experimental values (exp.). For the data points shown, the optimum λ_ε prefactor was used (see text in sect. 2.2.1), which is indicated by the labels. In (b) the results for the fluorides (for both F4 and F5 force fields) are depicted for various (including the optimum) λ_ε and λ_σ prefactors (see text in sect. 3.3). The lines correspond to the experimental data. The labels denote the scaling prefactors in each case. The color coding in (b) corresponds to the KF and NaF cases, respectively. All data are given for a 0.3 m (0.3 M) concentration.

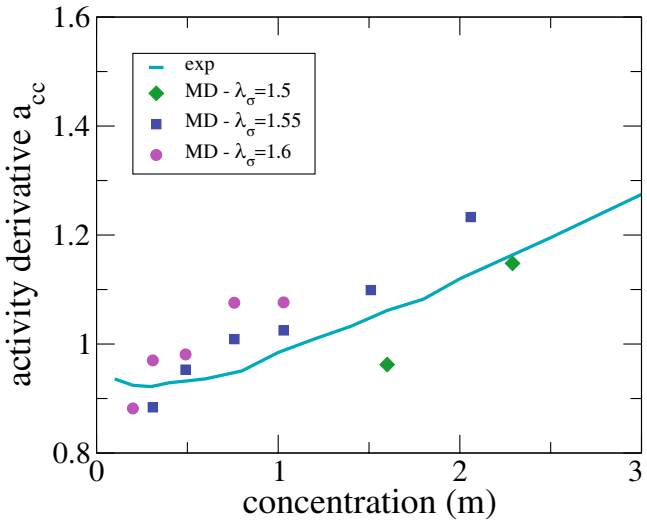

Fig. 8. Variation of the activity derivatives a_{cc} of the KF5 solution with concentration (m) and various λ_σ scaling prefactors.

for the concentration dependence of the activity derivatives are given in fig. 8. We took three different λ_σ values, which correspond to a_{cc} values very close to the crossing points with the experimental line (see fig. 4 in [19]) and consider relatively low concentrations, up to 2.5 m. From fig. 8 it is clear that small variations in the λ_σ lead to non-negligible differences in the calculated a_{cc}. It seems that $\lambda_\sigma = 1.55$ follows better the experimental variation of a_{cc} with concentration. However, for small concentrations (below 0.5 m), $\lambda_\sigma = 1.6$ can also be considered as a good choice for a good force field. The respective data for $\lambda_\sigma = 1.6$ start to deviate significantly for higher concentrations. For these concentrations, the choice of $\lambda_\sigma = 1.5$ leads to a_{cc} values which approach better the experimental line. The aim, here, was not to investigate the concentration dependence in all its detail, but only make the point that different scaling prefactors in the ion-pair mixing rules can lead to better optimized ionic force fields in different regions of the ionic concentrations. Which exactly are these prefactors need to be addressed separately for each salt solution. In this work, we only provide a guideline how to modify the ion-pair combination rules to generate good classical potentials for ions. The bottomline is that one needs to be accurate enough in the predictions and consistent with the ionic force field choice before applying it to specific systems under certain conditions.

4 Summary and conclusions

In conclusion, we have used Molecular Dynamics simulations to model salt solutions in water. We make use of our previously proposed optimization scheme for classical ionic force fields, which involved modified mixing rules, either for the cation-anion interaction of the cation-anion

effective radius. The Kirkwood-Buff theory of solutions are applied to link the structural details of the solution to its thermodynamic properties and provide a comparison to experimental data. Here, we provide a structural analysis of features such as the radial distribution functions, the short-ranged potentials of mean force, and the Kirkwood-Buff integrals. Specifically, our aim was to unravel the way these are affected by the scaling factors of the modified cation-anion mixing rules. Different representative salt solutions, also of biophysical interest, are investigated with a focus given on two of the fluorides, KF and NaF. The fluorides have been proven more difficult to optimize, possibly due to the small excess polarizability of F^- [39].

Here, we have first looked at the structural modifications of the radial distribution functions and the short-ranged pair potentials of the salt solutions due to the modified mixing rules. We underlined the dependence of the first ion-pair and second solvent-separated ion-pair peaks in the RDFs on the scaling prefactors of the ion-pair mixing rules. These also lead to a different bonding environment for the ion-pair, as monitored through the short-ranged potentials of mean force. A similar analysis was made for the different contributions to the KBIs and their respective structural modifications with the ion-pair distance. In general, values of either λ_ε or λ_σ below 1 lead to an unphysical stronger attraction between the cation and the anion, thus crystallization. This is clear from the very high peaks in the RDFs, the deeper potentials wells in the short-ranged potentials of mean force and the high absolute values in the KBIs. The different structure of the corresponding curves indicate the different bonding environments for the ion-pair for different λ_k values.

For the fluorides, we have used two previously optimized force fields for the F^- [12]. The comparison of the different F^- force fields and the different mixing rules prefactors to the corresponding experimental data for the activity derivatives reveals the optimum LJ parameters that apply to KF and NaF. It was shown that a different LJ parameter set is better applicable to different salt solutions. It is also clear from our analysis that, indeed also for NaF, use of the λ_σ scaling instead of λ_ε can lead to a crossover with the experimental data, thus a well-optimized force field. This was the case also for KF. In this way, we have confirmed that essentially both optimization techniques, use of modified cation-anion LJ interaction (through λ_ε) or LJ effective radius (through λ_σ) has the potential to derive well-optimized ionic force fields.

Specifically, though the optimization scheme based on λ_ε can be quite efficient for many salts, taking λ_σ as a variable allows more room for improvement. This is viewed with respect to the fact that the calculated a_{cc} variation with λ_σ always crosses the experimental line, as mentioned in this work. This inherently allows for an almost perfect match to the experimental results for a specific λ_σ. Hence, obtaining a well-optimized ionic force field seems much more straightforward than when modifying ε_{+-}. In all cases, for which we have modified the σ_{+-} mixing rule, we have seen exactly the same behavior: a continuous increase of the activity derivatives with λ_σ and a crossover with the experimental data. In essence, varying the effective LJ ion-pair radius does not allow the ion-pair to be trapped into a local minimum of the potential (as commonly occurs when ε_{+-} is modified) and leads to monotonically increasing thermodynamic properties from values below to over the experimental ones. This holds for both monovalent [19] and divalent [40] salts.

Finally, we have briefly touched the issue of the transferability of the ionic force fields considered in this work with concentration. We probe this for the KF case and the modified cation-anion effective LJ radius, for which we have shown that different λ_σ prefactors could be more effective at different concentration regions. In this respect and along the lines proposed here, care should be taken in choosing the correct mixing rules and their scaling prefactors for specific systems under certain conditions. Taking into account the above analysis, this work provides more insight into the subject of ionic force field optimization with modified mixing rules and the inherent structural changes in the bonding environment of the ion-pair within the solution. Note, as a general remark, that the present optimized potentials and λ_k values are designed to be used with the SPC/E water model, but other simple point charge models could also provide similar results [2]. What remains to be checked though is how the proposed ionic potentials will change if more complex water models are used under different conditions. It is expected that, in such cases, only the modification of the ion-pair mixing rules with the correct scaling prefactor and the existing ionic force fields should be sufficient for an efficient modeling of the respective system. In this respect, there would be no need to resort to new techniques for optimization of additional force fields.

The author is grateful to Roland R. Netz for his advice and guidance. Financial support from the "Gender Issue Incentive Funds" of the Cluster of Excellence in Munich, Germany and the "BioFuS" project of the Intra-European Marie-Curie Programm (call FP7-PEOPLE-2009-IEF) is greatly acknowledged.

References

1. D.E. Smith, L.X. Dang, J. Chem. Phys **100**, 3757 (1994).
2. S. Weerasinghe, P.W. Smith, J. Chem. Phys. **119**, 11342 (2003).
3. B. Hess, C. Holm, N. van der Vegt, Phys. Rev. Lett. **96**, 147801 (2006).
4. D. Frenkel, B. Smit, *Understanding Molecular Simulations* (Academic Press, New York, 1996).
5. B. Alberts, A. Johnson, J. Lewis, M. Raff, K. Roberts, P. Walter, *Molecular Biology of the Cell* (Garland Science, New York, 2002).
6. A. Savelyev, G.A. Papoian, J. Phys. Chem. B **112**, 9135 (2008).
7. T.M. Chang, L.X. Dang, Chem. Rev. **106**, 1305 (2006).
8. P. Jungwirth, D.J. Tobias, Chem. Rev. **106**, 1259 (2006).
9. I.S. Joung, T.E. Cheatham III, J. Phys. Chem. B **112**, 9020 (2008).

10. D. Horinek, S. Mamatkulov, R.R. Netz, J. Chem. Phys. **130**, 124507 (2009).
11. A.P. Lyubartsev, A. Laaksonen, Phys. Rev. E **55**, 5689 (1997).
12. M. Fyta, I. Kalcher, L. Vrbka, J. Dzubiella, R.R. Netz, J. Chem. Phys. **132**, 024911 (2010).
13. J.G Kirkwood, F.P. Buff, J. Chem. Phys. **19**, 774 (1951).
14. P.G. Kusalik, G.N. Patey, J. Chem. Phys. **86**, 5110 (1987).
15. R. Chitra, P.E. Smith, J. Chem. Phys. **114**, 426 (2001).
16. R. Chitra, P.E. Smith, J. Chem. Phys. **106**, 1491 (2002).
17. S. Weerasinghe, P.W. Smith, J. Chem. Phys. **118**, 10663 (2003).
18. D. Horinek, R.R. Netz, J. Phys. Chem. A **115**, 6125 (2011).
19. M. Fyta, R.R. Netz, to be published in J. Chem. Phys. **136**, issue 11 (2012).
20. B. Hess, N.F.A. van der Vegt, Proc. Natl. Acad. Sci. U.S.A. **106**, 13296 (2009).
21. M.B. Gee *et al.*, J. Chem. Theor. Comput. **7**, 1369 (2011).
22. H.J.C. Berendsen, D. van der Spoel, R. van der Drunen, Comput. Phys. Commun. **91**, 43 (1995).
23. E. Lindahl, B. Hess, D. van der Spoel, J. Mol. Mod. **7**, 306 (2001).
24. H.J.C. Berendsen, J.P.M. Postma, W.F. van Gunsteren, A. DiNola, J.R. Haak, J. Chem. Phys. **81**, 3684 (1984).
25. H.J.C. Berendsen, J.R. Grigera, T.P. Straatsma, J. Phys. Chem. **91**, 6269 (1987).
26. U. Essmann, L. Perera, M.L. Berkowitz, T. Darden, H. Lee, L.G. Pedersen, J. Chem. Phys. **103**, 8577 (1995).
27. D. Frenkel, B. Smit, *Understanding Molecular Simulation: From Algorithms to Applications* (Academic Press, 1996).
28. L.X. Dang, J. Am. Chem. Soc. **117**, 6954 (1995).
29. L.X. Dang, J. Chem. Phys. **96**, 6970 (1992).
30. I. Kalcher, J. Dzubiella, J. Chem. Phys. **130**, 134507 (2009).
31. A.P. Lyubartsev, S. Marčelja, Phys. Rev. E **65**, 041202 (2002).
32. J.E. Mayer, *Equilibrium Statistical Mechanics* (Pergamon, Oxford, 1968).
33. W.G. McMillan, J.E. Mayer, J. Chem. Phys. **13**, 276 (1945).
34. J.P. Hansen, I.R. McDonald, *Theory of Simple Liquids*, 2nd edition (Academic Press, London, 1986).
35. A. Ben-Naim, *Statistical Thermodynamics for Chemists and Biochemists* (Plenum, New York, 1992).
36. C.J. Fennell, A. Bizjak, V. Vlachy, K.A. Dill, J. Phys. Chem. B **113**, 6782 (2009).
37. J.J. Molina, J.-F. Dufréche, M. Salanne, O. Bernard, P. Turq, J. Chem. Phys. **135**, 234509 (2011).
38. R.A. Robinson, R.H. Stokes, *Electrolyte Solutions*, 2nd edition (Dover, New York, 2002).
39. R.R. Netz, Curr. Opin. Colloid Interface Sci. **9**, 192 (2004).
40. S. Mamatkulov *et al.*, unpublished data.